PRAMANA
— journal of
physics

Vol. 76, No. 2
February 2011
pp. 293–312

X-ray fluorescence activities at Saha Institute of Nuclear Physics, India

MANORANJAN SARKAR
Saha Institute of Nuclear Physics, 1/AF Bidhan Nagar, Kolkata 700 064, India
E-mail: manoranjan.sarkar@saha.ac.in

Abstract. This paper covers different aspects related to X-ray fluorescence activities at Saha Institute of Nuclear Physics, Kolkata, India. In its first part, experiments on basic physical problems are illustrated and in the second part, some applications related to X-ray fluorescence are discussed.

Keywords. X-ray fluorescence; energy-dispersive X-ray fluorescence; cross-sections; satellites; anisotropy; Coster–Kronig parameter; archaeology; environment.

PACS Nos 32.80.-t; 78.70.En

1. Introduction

X-ray fluorescence activities at Saha Institute of Nuclear Physics are pursued around three facilities that we have in our division: (i) a Kevex 60 W X-ray generator, (ii) a curved crystal spectrometer (Spectroscan VY) and (iii) ^{109}Cd and ^{241}Am radioactive sources.

With the Kevex X-ray generator, using an XYZ geometry, different secondary targets are used to get almost monochromatic X-rays for measuring X-ray production and elastic scattering cross-section of different elements. The curved crystal spectrometer is totally devoted to the measurements of satellite and hypersatellite lines from pure as well as compounds excited by the tube bremsstrahlung from a 40 W X-ray tube built-in within the spectrometer. A ^{109}Cd source is used to excite K and L X-rays from pure foil and these X-rays are then measured in coincidence to obtain the value of f_{23} parameter. The angular distribution of L X-rays excited by the same source is measured over different angles to give a decisive answer to the ambiguity that exists in the angular distribution measurements.

As far as the application part of X-ray fluorescence is concerned, an energy-dispersive X-ray fluorescence (EDXRF) system was developed to analyse alloys by exposing them directly under the tube bremsstrahlung and also under monochromatic X-rays obtained from secondary targets. In both the cases, no standard sample is required. Using the above principle, some archaeological objects were analysed. Another EDXRF set-up with the radioactive sources is made available where long exposure of the samples are required.

Environmental samples such as municipal solid waste (MSW), soil evolved from MSW, vegetables grown on these soils etc. were analysed with this set-up.

2. Experiments on basic physical problems

2.1 *L X-ray fluorescence cross-section measurements*

X-ray fluorescence cross-section data are used as important inputs in atomic, molecular and medical physics and also in X-ray fluorescence technique. As far as K X-ray fluorescence cross-sections are concerned, they were extensively studied and these cross-sections can now be theoretically predicted within a few percent. But L shell has three subshells and each subshell has different sets of atomic parameters. The theoretical values of these parameters differ widely among themselves which are reflected in the theoretical L X-ray fluorescence cross-section values. So, instead of using the theoretical values, measured values of the L X-ray fluorescence cross-sections, especially at low photon energies, are very much needed.

The set-up used for the measurement of L shell X-ray fluorescence cross-section is shown in figure 1. The 60 W Kevex X-ray tube was the main source of X-rays. Depending on the excitation energies, secondary targets were selected. Tube bremsstrahlung first fell on the secondary target producing characteristic X-rays of the secondary target to excite the sample (main target). L X-rays from the samples were detected by a Si(Li)/HPGe detector. Signals were then processed through a pulse processor and fed into a multichannel analyser. A typical spectrum of L X-rays from U is shown in figure 2.

The L shell X-ray fluorescence cross-section is obtained from the relation

$$\sigma_{\mathrm{L}}^{x} = \frac{N_x}{I_0 G \varepsilon m \beta}, \tag{1}$$

where σ_{L}^{x} is the L shell X-ray fluorescence cross-section, N_x is the peak integral under a particular L line, I_0 is the incident flux on the sample, G is the geometrical factor between the sample and the detector, ε is the efficiency of the detector at a particular energy, m

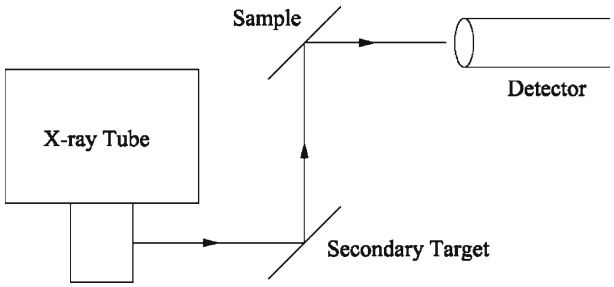

Figure 1. A schematic experimental set-up for cross-section measurement.

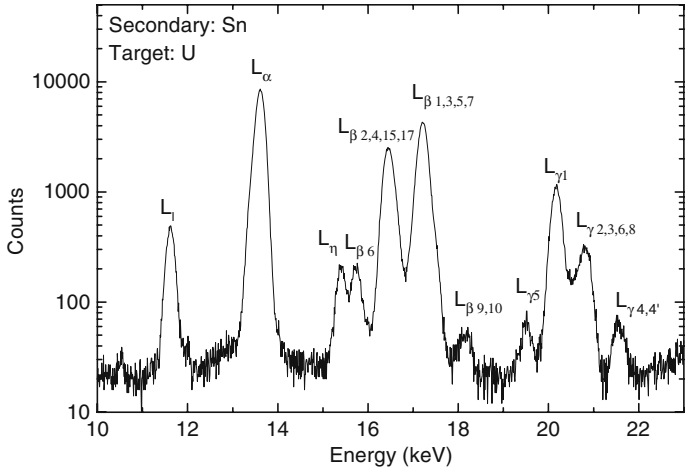

Figure 2. A typical L X-ray spectrum of U irradiated with K X-rays of Sn. The X-ray tube was run at 40 kV with a current of 0.1 mA.

is the thickness of the sample in g/cm^2 and β is the absorption correction factor for the incoming and outgoing X-rays from the sample which is given by

$$\beta = \frac{1 - \exp\left[-(\mu_{\text{in}}/\sin\psi_1 + \mu_{\text{em}}/\sin\psi_2)\right] m}{\left[\mu_{\text{in}}/\sin\psi_1 + \mu_{\text{em}}/\sin\psi_2\right] m}, \tag{2}$$

where μ_{in} and μ_{em} are the total mass absorption coefficient of the sample for the primary and fluorescence X-rays respectively, ψ_1 and ψ_2 are the incident and emergent angles respectively.

Using the same experimental set-up and varying the secondary targets, L shell X-ray fluorescence cross-sections of (i) Au and Pb at 21.6, 23.7 and 25.8 keV, (ii) rare earth elements ($Z = 62$, 64, 66, 68 and 70) at 17.8, 22.6 and 25.8 keV and (iii) Th and U at 22.6, 25.8 and 32.9 keV were measured. Theoretical photoionizaion cross-sections of Scofield [1] were then converted to X-ray fluorescence cross-sections using the values of atomic parameters from different sources [2–6]. It was observed that if the Scofield photoionization cross-sections are converted to X-ray fluorescence cross-sections taking the values of fluorescence yield and Coster–Kronig parameters from Puri [5] and the radiative widths from Campbell and Wang [3], the experimental values of L X-ray fluorescence cross-sections of Au and Pb are within 10% of the theoretical predictions while those of the rare earth elements are within 5%. But for Th and U the deviation is larger, the data lie within 30%.

2.2 *Determination of Coster–Kronig transition probability (f_{23})*

Methods for the measurements of atomic parameters can be broadly classified into two: (1) single spectrum method and (2) coincidence method. In single spectrum method,

the precision of the measurements cannot be brought down below a few percent while in the latter, it can be brought down even less than 1%. In coincidence experiments [7–10], radioactive targets are used but for all elements, it is difficult to get the long-lived radioactive targets. The alternative way will be to excite a sample with a suitable radioactive source whose excitation energy is very close to the K shell binding energy of the element. The emitted K and subsequently emitted L X-rays can be measured in coincidence to get high precision values of atomic parameter.

It can be shown [8] that the value of f_{23} can be obtained from the relation (when the angle between the K and L X-ray detector is 125°)

$$f_{23} = \frac{C(\mathrm{L}_\alpha, \mathrm{K}_{\alpha 2})n(\mathrm{K}_{\alpha 1})}{C(\mathrm{L}_\alpha, \mathrm{K}_{\alpha 1})n(\mathrm{K}_{\alpha 2})}, \tag{3}$$

where $C(\mathrm{L}_\alpha, \mathrm{K}_{\alpha 2})$ and $C(\mathrm{L}_\alpha, \mathrm{K}_{\alpha 1})$ are the L_α coincidence events gated by $\mathrm{K}_{\alpha 2}$ and $\mathrm{K}_{\alpha 1}$, $n(\mathrm{K}_{\alpha 1})$ and $n(\mathrm{K}_{\alpha 2})$ are the corresponding events of $\mathrm{K}_{\alpha 1}$ and $\mathrm{K}_{\alpha 2}$. The right-hand side of eq. (3) is only the numbers and so the error in f_{23} can be brought down below 1% if statistics of the numbers C and n are improved.

In our laboratory, 88 keV γ-rays emitted from a 2 mCi ^{109}Cd source was used to excite the K shell of Au (K shell binding energy = 80.72 keV). A 53.7 mg/cm^2 Au pure foil was used as a target. The experimental arrangement of the set-up is shown in figure 3. K X-rays ($\mathrm{K}_{\alpha 1}$ and $\mathrm{K}_{\alpha 2}$) from Au were detected with an ORTEC LEPS (HPGe) detector while the L X-rays were detected with a DSG Si(Li) detector. Two detectors were placed at angle of 125° so as to eliminate the angular correlation effect between K and L X-rays.

The software INGASORT, developed by the Nuclear Science Centre, New Delhi was used to analyse data event by event in list mode. A detailed description of the analysis of these data is given in [11]. Using the relation (3), the value of f_{23} was found to be 0.119 $\pm$ 0.003. The other measured values were 0.100 $\pm$ 0.009 [12], 0.101 $\pm$ 0.010 [13], 0.125

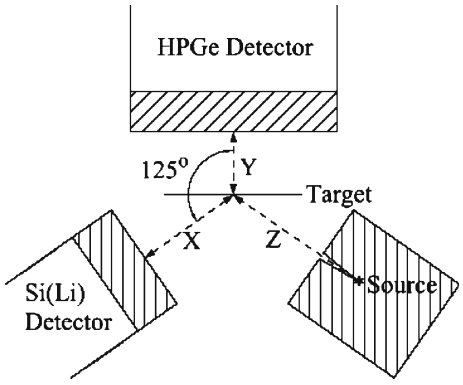

Figure 3. A schematic diagram of the coincidence experimental set-up. $X = 20$ mm, $Y = 40$ mm, $Z = 3$ mm (distances are not to scale).

$\pm$ 0.013 [14]. Our measured value was lying above the values determined by synchrotron [12,13] but very close to the semi-empirical value of Krause [2] and slightly less than the relativistic value calculated by Chen *et al* [15].

Present method is a general one. With a suitable X-ray source, K shell of any element can be excited to get K and subsequently L X-rays to carry out such coincidence experiment. In this measurement, a weak radioactive source was used and the data were collected over 60 days to get the value of f_{23} with an error of 2.5%. But if the data were collected with a stronger source over a longer period, the error in the measurement could be brought down even less than 1%.

2.3 *Studies of satellites, hypersatellites and radiative Auger emission*

Satellite lines appear when an electronic transition occurs in an atom in the presence of spectator vacancies. For example, an electronic transition from L to K shell in the presence of single vacancy in the L shell will give rise to the first K satellite denoted by KL^1 whose energy will be slightly higher than the main diagram line KL^0. Similarly, depending on the number of vacancies in the L shell, the second, third, fourth, etc. satellites can be represented by KL^1, KL^2, KL^3, and so on. Removal of an electron from an inner shell reduces the screening of the atomic potential. Because of this, the binding energies of the inner shells are increased more than that of the outer shells. So a photon emitted from a multiply ionized atom because of the electronic transition from the outer to the inner shell will have slightly higher energies than the normal diagram line. Beside the KL^n (n = 1,2,3, ...) satellites, there is also another type of satellite called 'hypersatellite' which occurs when the inner shell of an atom has two vacancies.

A vacancy created in the inner shell can decay either through a radiative or a non-radiative process. In the non-radiative process, it is normally assumed that instead of emission of the characteristic radiation, another electron from the same or higher shell is ejected with the kinetic energy equal to the non-emitted characteristic radiation minus the binding energy of the shell/subshell from where the electron is ejected. But there might be another possibility where the energy of the electron is shared between the electron and a photon. Mathematically it can be written as

$$h\nu = E(KLM) - E_e(M), \tag{4}$$

where $h\nu$ is the energy of the emitted photon due to radiative Auger emission (RAE), $E(KLM)$ is the full energy of the Auger electron if there had been no photon emission and $E_e(M)$ is the actual energy of the emitted Auger electron. From the above equation, it is clear that the radiative energy of the RAE photon can go from 0 to a maximum of $E(KLM)$.

Here, we shall report on the satellite, hypersatellite and RAE structures of a few elements excited by the bremsstrahlung from an Ag anode. The peak shifts of these lines with respect to their parent lines will be compared with other available data and also with our Multi-Configuration Dirac–Fock (MCDF) calculations.

'Spectroscan VY' manufactured by Spectron-OPTEL RMA Inc. Russia was used for the present measurements. Detailed description of the instrument and the measurement procedure are described in our earlier publication [16]. Among the four crystals, LiF was selected for this measurement. At the start of the experiment, the energy calibration of the system was done by detecting the K_α lines from Cr, Ti, Ca, Cl, S, P and Si obtained from the two standards supplied by the manufacturer. The Ag X-ray tube was run at 35 kV with a current of 40 μA. Pure foils of Ti, V and Fe imported from Goodfellow, UK were used as the respective targets. For the Mn sample, an alloy of Mn–Ni and for the Cr sample, a pellet of Cr_2O_3 were used. All the samples were exposed to the bremsstrahlung of the Ag anode keeping the foils/pellet on the built-in target holder.

A typical structure of satellites, hypersatellites and RAE structures from Cr is shown in figure 4. To avoid any error in citing the peak positions, we had rather determined the shifts of these satellite lines with respect to their respective parent lines. One such example is shown in figure 5 where the energy shifts for $K_\alpha L^2$ are displayed. Our data are compared with the data of others and with our MCDF calculations. MCDF values showed reasonable agreement with our data.

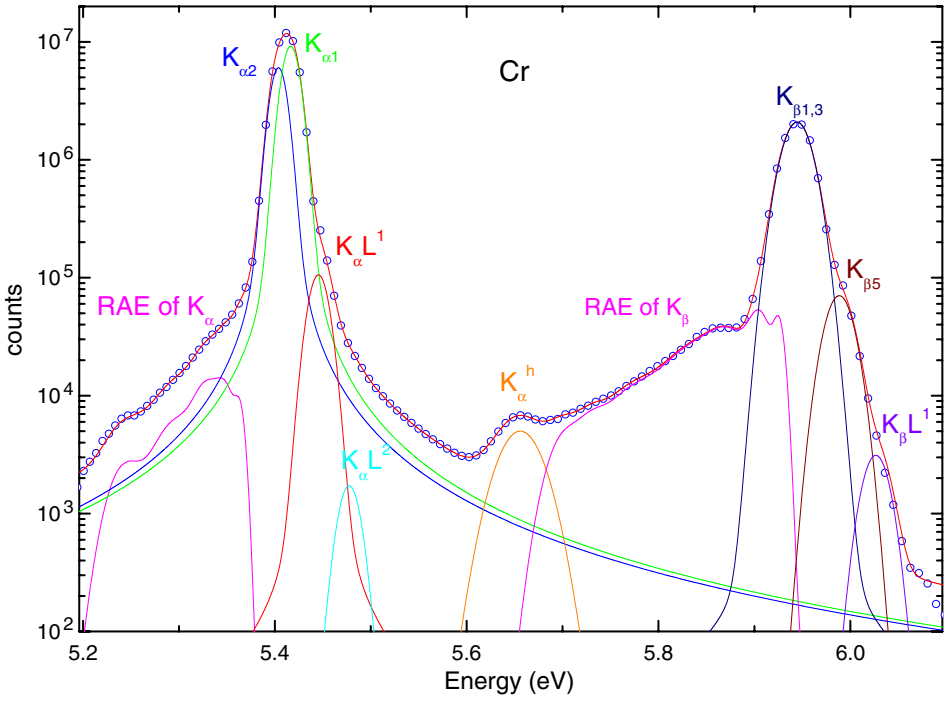

Figure 4. Deconvoluted satellite, hypersatellite and RAE structures of the background-substracted spectrum of Cr.

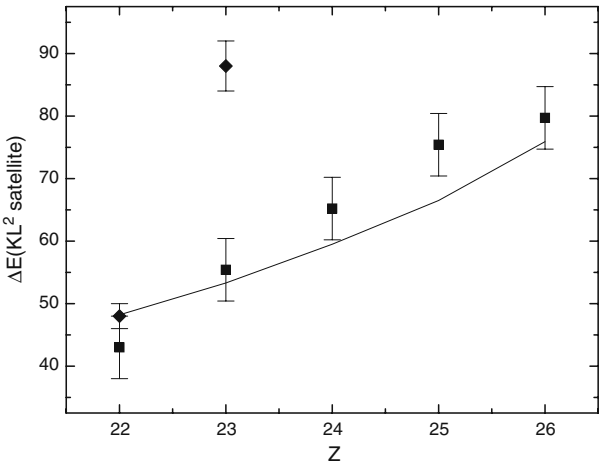

Figure 5. Energy shift (eV) of $K_\alpha L^2$ satellite with respect to K_α line. (■) present data, (♦) Verma [61] and (—) our MCDF.

2.4 *Angular distribution of Au and U L X-rays induced by 22.6 keV photons*

It is now a well-established fact that when charged particles (protons, electrons, heavy ions) produce vacancies in atoms at energy levels with $J > 1/2$, the resulting ions will be aligned. The signature of this alignment of ions is anisotropic angular distribution of the ejected Auger electrons/emitted characteristic radiation or the degree of polarization of the radiation. This anisotropic behaviour is caused by the nonstatistical distributions of different magnetic substates by the ionized atoms.

But in the case of photon-induced ionization, the situation is not very clear. Results of alignment studies of ions by measuring the angular distribution of the emitted characteristic radiation are still confusing. Data from different groups show contradictory results. The groups at Patiala, India [17–20] and in Turkey [21–28] got very strong anisotropy while the others [29–36] observed no anisotropy or very little anisotropy in their measurements. Moreover, it is observed that the theoretical value of the alignment parameter based on non-relativistic calculation of Berezhko *et al* [37] are 2–3 times higher than the experimental values of Küst *et al* [35], almost five times larger in the case of Papp and Campbell [29] and about half of the experimental values of Yamaoka *et al* [34]. So, the contradiction exists not only on the existence of anisotropy in emission of the L X-rays but also on the magnitude of the alignment parameter of the ions.

To throw some light on these issues, we have used a ^{109}Cd source to ionize Au and U foils and then measured their L X-rays at different angles. With these measurements, efforts were made to check (i) if L X-rays were isotropic or not, and if so, (ii) to obtain the values of the anisotropy and alignment parameters.

A ^{109}Cd point source of strength 30 mCi was used to excite the L X-rays from the targets. Both the target and the exciting source were fixed and the Si(Li) detector used

to detect the L X-rays was placed on a movable stand. The angular coverage in this experiment was 70–150° with respect to the direction of the exciting X-rays from the source. The source was kept in a graded collimator made of Al, Cu and Pb with an exit diameter of 2 mm. It was set at an angle of 60° with respect to the normal to the target. The ORTEC Si(Li) detector used in this experiment had an energy resolution of 160 eV at 5.9 keV. All the signals were collected in a PC fitted with an OXFORD MCA card. Two targets – (a) Au foil (54 mg/cm^2) and (b) U foil (194 mg/cm^2) – were used in this experiment.

The misalignment of the angular distribution table was checked with a ^{241}Am source and found to be within 2%. This signifies that with our system, an isotropy of 2% or less cannot be measured.

Peak integrals of all L lines were corrected for self-absorption and then plotted against the measured angles. A typical plot for L_l line from Au is shown in figure 6. It was observed that the intensities of all the L lines are almost isotropic contrary to the observation of Kahlon *et al* [17–20], Ertugrul *et al* [21–23], Demir *et al* [24,27] and Seven *et al* [25,26,28].

Assuming the emission of X-rays as electric dipole in nature, the normalized intensities of L lines were plotted against $P_2(\cos\theta)$ to get the anisotropic parameter (β) of main L lines. From the β value of L_l lines [38], the alignment parameter of Au was found as to 0.10 ± 0.14, while for U no effort was made to calculate the alignment parameter as the anisotropic parameter was almost equal to the misalignment of our set-up.

The two major observations in our study were (i) our angular distribution data did not show any sharp decrease with the increase of angle as was observed by the group of Patiala and Turkey, whereas it showed almost isotropic behaviour as observed by [29–34], and (ii) the alignment parameter of Au was very small.

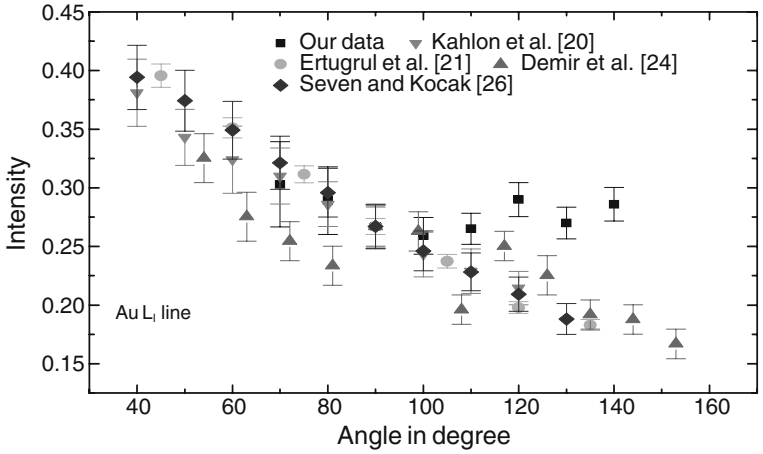

Figure 6. Plot of the intensity of L_l line of Au against different measuring angles. Normalized intensities of other groups are also shown.

2.5 *Measurements of differential elastic scattering cross-sections*

In elastic scattering, the incident photon is deflected but retains the same energy with which it was incident on the target. The contributions to this elastic scattering may come either from (i) the bound electrons, when the process is called Rayleigh scattering, or from (ii) the nucleus. In the energy range of our interest ($E = 22.1$ keV) the Rayleigh scattering will be the predominant mode. The major basic theoretical approaches developed for Rayleigh scattering are the non-relativistic form factors (NFF), relativistic form factors (RFF), modified relativistic form factor (MRFF), relativistic form factor with anomalous scattering correction (RFFASF), modified relativistic form factor with anomalous scattering correction (MRFFASF) [39–45] and the state-of-the-art S matrix calculations [46–48].

To our knowledge, there exists only one such measurement [49] with present combination of energy (22.1 keV) and angle (90°). Our particular choice of this energy for the present measurement stems mainly from the fact that (a) with our set of targets, we would be able to investigate the so-called edge effect with Nb ($E_k = 18.9986$ keV), Mo ($E_k = 19.9995$ keV) and Pd ($E_k = 24.3503$ keV) and (b) in most of the X-ray fluorescence laboratories, the exciting source is either ^{109}Cd ($E_{K_\alpha} = 22.1$ keV) or ^{241}Am ($E_\gamma = 59.54$ keV).

The experimental arrangement of the present measurement is the same as shown in figure 1. Here, a silver foil was used as a secondary target. Spectroscopically pure foils of Ti, V, Fe, Ni, Cu, Zn, Zr, Nb, Mo, Pd, Cd, In, Sn, Sm, Gd, Dy, Er, Yb, Au and Pb were used as targets. An ORTEC LEPS (HPGe) used to detect X-rays had a resolution of 170 eV at 5.9 keV. The X-ray tube was run at 40 kV with a current of 0.2 mA. A typical spectrum of Pb is shown in figure 7. The differential elastic scattering cross-section at a particular angle θ (here $\theta = 90°$) is obtained using the relation

$$\left(\frac{\mathrm{d}\sigma}{\mathrm{d}\Omega}\right)_{\mathrm{el}} = \frac{N_{\mathrm{el}}}{4\pi I_0 G \varepsilon_{\mathrm{el}} m \beta}, \tag{5}$$

where N_{el} is the number of counts under the elastic peak, I_0 is the incident flux, G is the geometry factor, $\varepsilon_{\mathrm{el}}$ is the efficiency of the detector at the elastic peak energy, m is the real density of the target in g/cm^2 and β is the absorption correction factor for the incident and elastically scattered radiation inside the target and is evaluated using eq. (5) [50].

While comparing our data with different theoretical predictions, it was revealed that

(a) For the low Z elements ($Z = 22$–40) present data were in general higher (∼7%) than the predictions of NFF, RFF and MRFF but lower (∼3%) than the RFFASF, MRFFASF and S matrix predictions.
(b) For elements ($Z = 41$, 42 and 46) having K edges close to the excitation energy, the data were always high compared to any existing theories. For $Z = 42$ where the difference between the K absorption edge and the exciting radiation was the minimum (2.1 keV) the measured value of cross-section was almost 30% higher than the S matrix calculations and for $Z = 41$ this factor was 16%. For $Z = 46$, the experimental value was 25% lower than the predictions of NFF, MRFF and RFF, but higher by 8% than the S matrix, RFFASF and MRFFAS calculations. As suggested by Jung *et al* [51], this mismatch of the measured elastic scattering cross-sections with the S matrix predictions near the K absorption edges might be

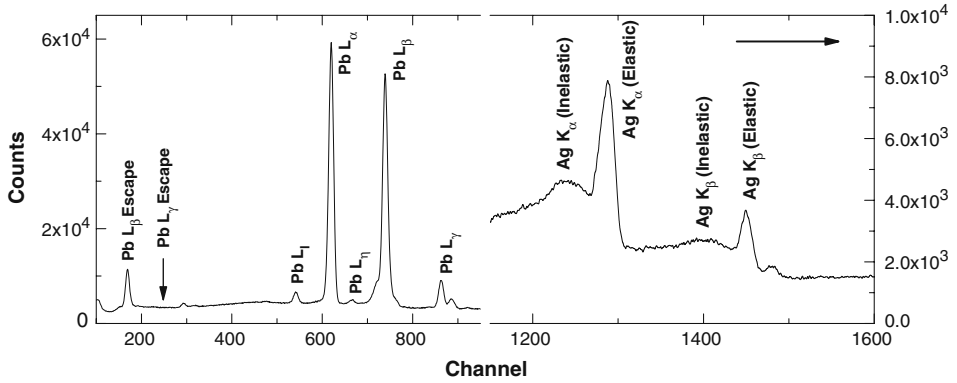

Figure 7. The full spectrum of Pb target excited by 22.1 keV X-rays obtained from an Ag foil used as the secondary target.

due to the non-local exchange effect and electron correlation which have not been included even in the state-of-the-art S matrix calculation.

(c) For $Z = 48, 49$ and 50, the data were lower by 4% than the predictions of S matrix, RFFASF and MRFFASF, and 22% lower than those of NFF, MRFF and RFF.

(d) For high Z elements ($Z = 62$–82) our data were closer to the predictions of NFF and MRFF (lower by 5%) and this deviation increased to 11% when compared to other theories.

3. Applications related to X-ray fluorescence

Energy-dispersive X-ray fluorescence (EDXRF) technique is one of the most versatile, non-destructive techniques for quantitative analysis of various types of samples. Compared to other non-destructive techniques such as particle-induced X-ray emission (PIXE) or electron probe microanalysis (EPMA), it is less expensive and requires less space and technical effort to run such a system. In our Division, we have two radioactive sources (^{109}Cd and ^{241}Am), a 60 W X-ray tube, Si(Li) detectors, necessary pulse processing units, MCAs etc. With all these components, two EDXRF systems were developed – one with the 60 W X-ray tube for short exposure of samples mostly alloys and the other, with radioactive sources for long exposure of samples mostly environmental in nature.

3.1 *EDXRF system with X-ray tube*

Based on fundamental parameter method, a technique has been developed [52] to analyse alloys, old archaeological objects etc. using the 60 W X-ray tube. Secondary targets as well as direct tube bremsstrahlung are used to excite the samples. To check the performance of this system, two standard alloys (Mn-Ni alloy from Johnson Mathey & Co. Ltd. and a brass sample from NIST) have been analysed and the results are shown in table 1.

Table 1. Compositional analysis.

Element	Results (in wt%) with bremsstrahlung	Results (in wt%) with Mo secondary	Quoted (in wt%)
(a) Mn-Ni alloy			
Mn	86.7 ± 7.8	86.7 ± 7.8	88
Ni	13.3 ± 1.2	13.3 ± 1.2	12
(b) NIST brass			
Fe	0.10 ± 0.01	0.30 ± 0.03	0.088
Ni	0.10 ± 0.02	0.10 ± 0.02	0.07
Cu	63.9 ± 3.4	61.8 ± 6.2	61.33
Zn	34.1 ± 3.4	35.8 ± 3.6	35.31
Sn	Not detected	Not detected	0.43
Pb	1.8 ± 0.2	2.0 ± 0.3	2.77

As can be seen from this table, in both the cases, the elemental concentrations of the standards agree quite well with the quoted values when the elemental abundance is greater than 1%.

In collaboration with the Asiatic Society Kolkata, 85 Malhar coins (Malhar is situated at 21.0°N, 82.2°E, a region in the Bilaspur district of Chattisgarh State of India) from 1st century BC to 4th century AD were analysed with this system [53]. Some of the images of the coins are shown in figure 8.

From the analysis, the following observations were made:

1. The coins of the earlier era (up to 2nd/3rd century AD) were mostly of lead or with high lead percentage mixed with other metals like Fe, Cu and Zn. The possible reasons could be the easy availability of lead in this region, or that lead has a low melting point and hardens fast on cooling. These factors made it the most suitable metal for minting purpose.
2. The minimal occurrence of Fe, Cu and Zn in the Pb coins was possibly not due to any kind of alloying as these metals have not been mixed in any particular proportion. These were present in the ore in the form of natural contamination and the process of purification of the ore was either not known to the people of that area or they hardly paid any attention to the purity factor as these coins were for transaction only within the area of Malhar. With widening of transaction, people needed coins in a more durable metal and they started experimenting with harder metals like Cu mixed with Fe, Pb or Zn. This experimentation in the alloying process continued till they reached an approximate standard of 80–90% Cu with small admixture of the other metals mentioned above.
3. The presence of arsenic in some of the copper coins indicated that the Cu ore used in minting these coins came from a mine which had a natural contamination of arsenic.
4. In some coins Zn was added to Cu as the hardening factor of Zn was possibly known by then, and Pb was either added or was an impurity present in the Cu ore used for minting these coins.

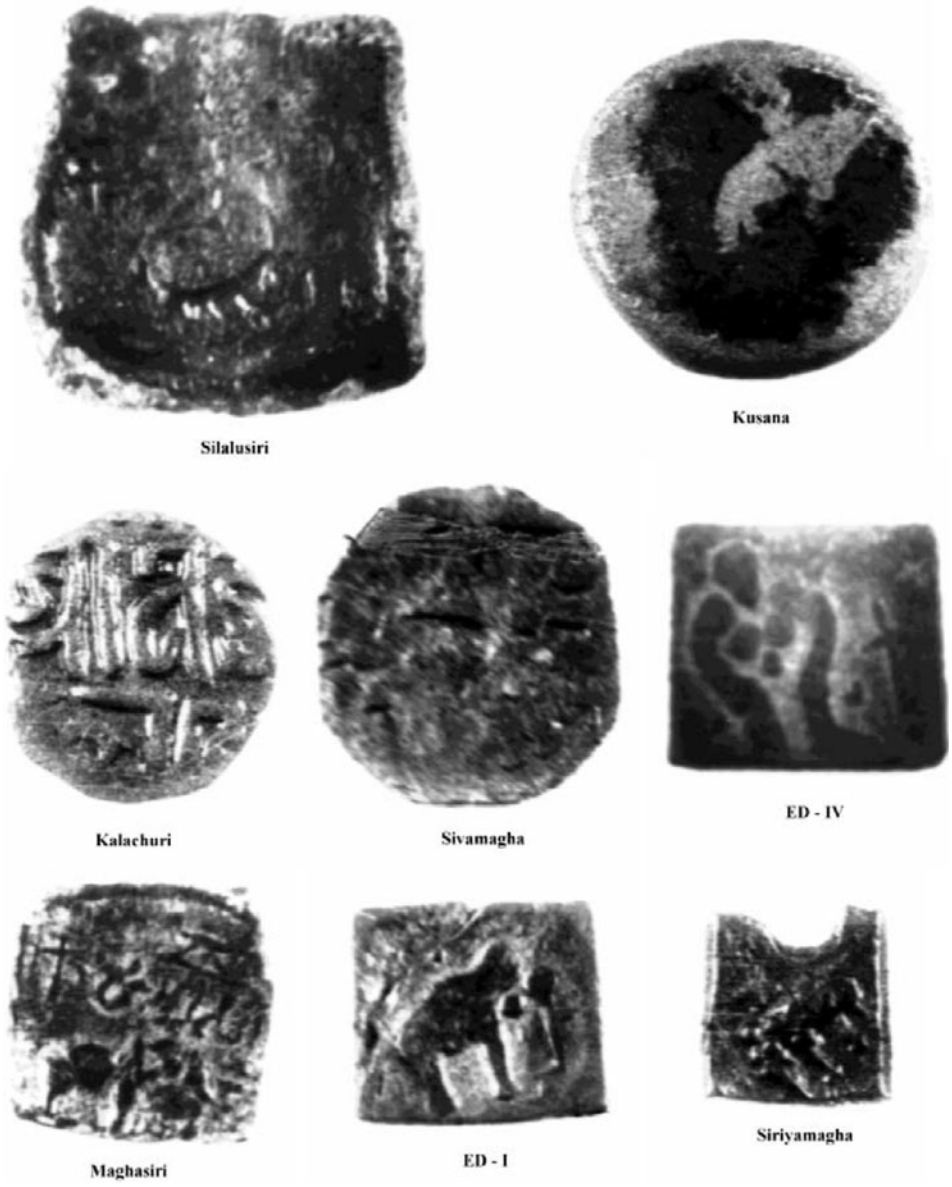

Figure 8. Some of the images of Malhar coins.

In another collaborative work with Centre for Archaeological Studies and Training, Kolkata, two sets of bronze images (4 Buddha, 11 Hindu images) from West Bengal Archaeological Museum were analysed [54]. Two images, one from each set, are shown in figure 9. The main aim of this analysis was to throw some light if the two sets of images

were fabricated from the same place and if the Buddha images were from Kurkihar, a place in Bihar state in India.

From the elemental analysis of these objects, it was concluded that

(1) Hindu images were homogeneous while Buddha images were highly non-homogeneous indicating that the places of origin of these two types of images were different.
(2) Although the stylistic pattern of the Buddha images were similar to those from Kurkihar, the presence of Sb (which is absent in Kurkihar images) suggested that these four Buddha images might have been made in a different place.

3.2 *EDXRF system with radioactive sources*

For the last couple of years, a collaborative work with the West Bengal Pollution Control Board has been carried out to analyse different types of environmental samples such

Figure 9. (**a**) Hindu image, (**b**) Buddha image.

as municipal solid waste (MSW) of different localities, soils collected from the MSW dumping site, vegetables grown on MSW soils, etc.

The separate EDXRF set-up used to analyse these samples consisted of a ^{109}Cd source, a Si(Li) detector with necessary electronics, a computer fitted with an ORTEC Maestro MCA card. The source and the sample were placed in an assembly as shown in figure 10 where graded collimators made of Bi, Cu and Al were used.

Most of the environmental samples are either powder or solid in nature. Powdered samples were first dried, ground in an agate mortar with pestle, and if necessary, mixed with a binder to make pellets in a pelletizer. Solid samples such as vegetables were first washed, then chopped and dried and made into pellets using the same technique.

Concentration of the ith element (in mg/g) in the sample is determined using the relation for the mass per unit area, m_i (in g/cm^2) [55]

$$m_i = (N_{E_i}/\mathrm{s})\ \{(\sigma_x \omega_x f_x)_i (I_0 G \varepsilon_{E_i}) \beta_{E_i}\},$$

where N_{E_i}/s is the number of counts corresponding to a particular X-ray energy (denoted by E_i) per unit time; σ_x is the photoionization cross-section of exciting radiation for K (or L) shell in cm^2/g for element i; ω_x, f_x are the fluorescence yield and branching ratio respectively of the fluorescent X-ray of the element I, I_0 is the incident flux; G is the factor depending on the geometry of the set-up; ε_{E_i} is the intrinsic efficiency of the detector and β_{E_i} is the absorption correction factor for incident (energy, E_0) as well as fluorescent

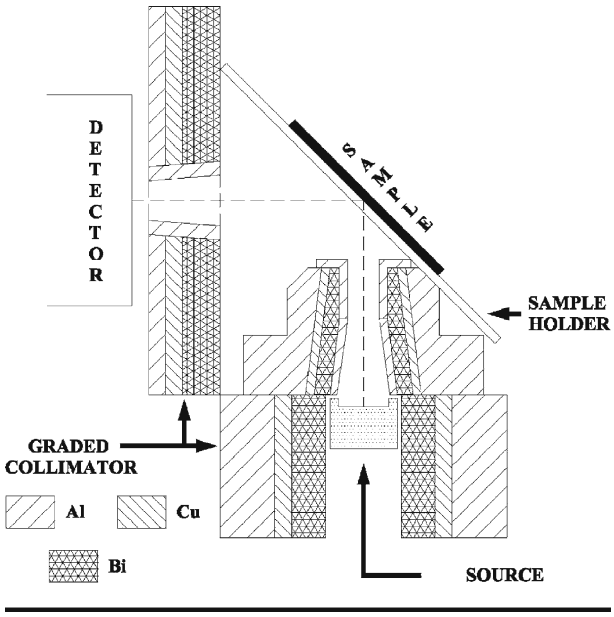

Figure 10. Experimental set-up of EDXRF system with radioactive source.

X-rays. In our earlier analyses, X-ray absorption factor was experimentally determined by emission transmission method [56] but later, QXAS code from IAEA, Vienna [57] was used to get the concentration values directly from that code where absorption correction was done with the help of coherent and incoherent peak intensities.

To check the reliability of such systems, a few standard samples from the National Institute of Standard and Technology (NIST) were analysed. A typical spectrum from one such standard is shown in figure 11. The compositional analysis of the standard agrees quite well with the cited values of NIST.

Few MSW samples of urban and suburban areas were subjected to EDXRF analysis [58]. A typical spectrum from the MSW of an urban area is shown in figure 12. From the compositional analysis it appeared that the nature of composition of all the samples were almost the same although the urban MSW contained three times higher value of Pb than that in suburban areas. It was also observed that the concentration level of all the elements starting from Ti to Pb except Fe was 2–7 factors higher than the ecological screening values while from Fe it varied from 100 to 200 times. Such high level of concentration of elements in the MSW is a grave concern to human beings as vegetables grown on the soils evolved from MSW might cause adverse effect on human bodies.

Six top soil samples were collected starting from near the present core MSW dumping site and ending near the bypass highway stretching a length of 2000 m. For comparison, soil samples (uncontaminated) from a village about 50 km from Kolkata were also collected. All these samples were then analysed with the EDXRF system. A typical spectrum

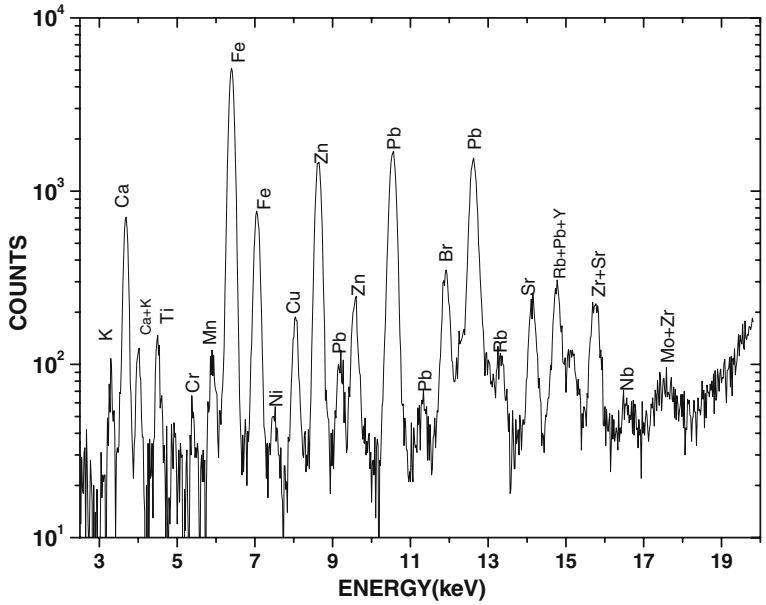

Figure 11. A spectrum from a standard (urban particulate matter, SRM no. 1648 from NIST).

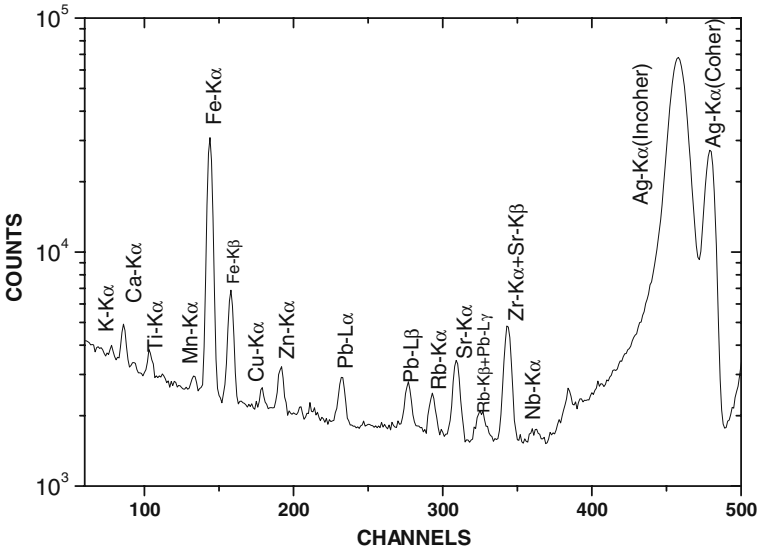

Figure 12. A spectrum from municipal solid waste.

from one of the top soil samples is shown in figure 13. It was observed that K, Ca and Fe were the major elements in all the MSW soil samples with an average concentration of 1.6, 2.7 and 4.7%, respectively, whereas the concentrations of these elements in the

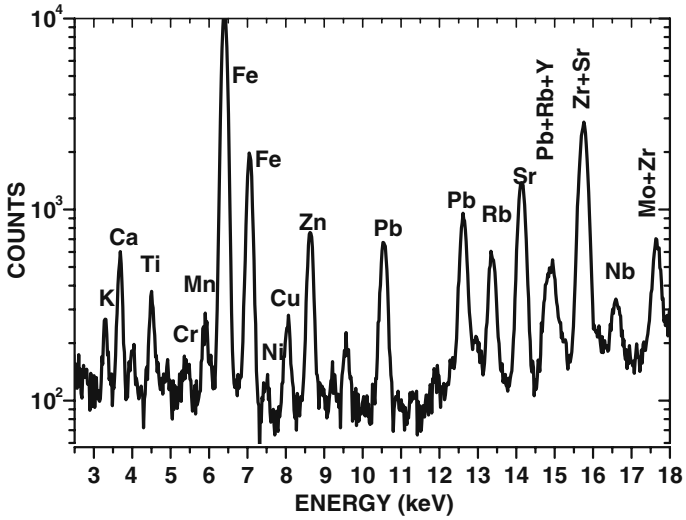

Figure 13. A spectrum from the top soil from the MSW dumping site.

country soil were 1.7, 0.7 and 2.3%, respectively. When the ratios of the concentration of elements in the soil sample of the dumping site to that in the village soil were compared, it was observed that the concentration levels of Ca and Cr were higher by four times; Ti, Mn, Fe and Sr by 2–3 times; Cu, Zn and Pb by an order of magnitude; and Pb in road side sample by two orders of magnitude. The concentration level of K, Rb and Zr remained the same. Unexpected high level of Pb in the roadside sample might be due to the vehicular movement along the road or the indiscriminate dumping of MSW. The high concentration of heavy metals in the top soil was due to the fact that this soil was evolved from the MSW which was highly contaminated with heavy elements. Vegetables grown on such soil are likely to contaminate the food chain.

To investigate the uptake pattern of the essential, non-essential and toxic elements in the vegetables grown on the MSW soil, a hyper accumulating plant species like radish was collected from an area where soils were evolved from the MSW of Kolkata City. Root soils, roots and leaves were analysed with the EDXRF system [59]. A spectrum from the radish leaf is shown in figure 14. It was observed that the concentration of Ti–Pd in the root soil was much higher than the ecological screening values. The concentration level of Ni, Cu, Zn and Pb in radish root and leaves were compared with those radish shoots grown on controlled soil [60]. It was observed that the concentration level was much higher in the present sample compared to the samples grown on the controlled soil. It was also observed that the accumulation of elements in the leaves was higher than in any other parts.

Cauliflowers were also collected from the MSW dumping sites in Kolkata and also from two villages about 50 km away from the city. As in the case of radish sample, here the root soil, leaves and the edible flower parts were analysed with the EDXRF system. A

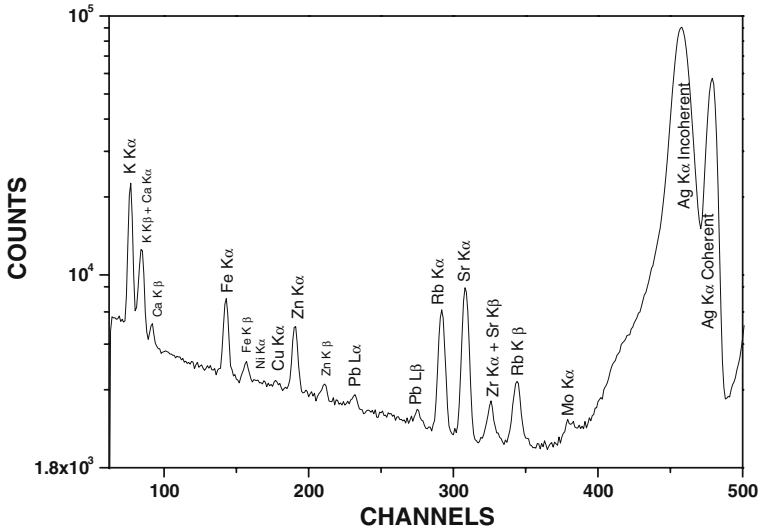

Figure 14. A spectrum from leaves of radish grown on MSW soil.

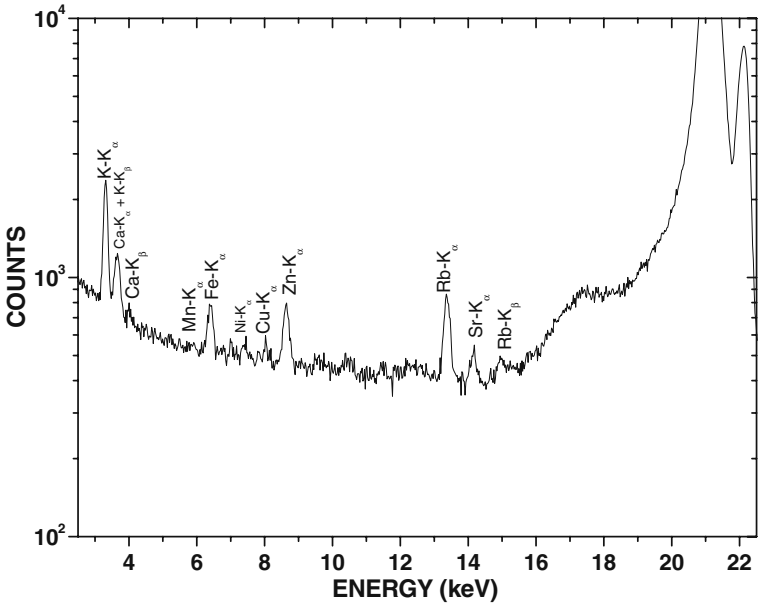

Figure 15. A spectrum from the edible part of the cauliflower grown on MSW soil.

spectrum from the flower part is shown in figure 15. Elements like Cr, Mn, Ni, Sr, Cu, Zn and Pb were higher in the root soil samples of the dumping sites than in the uncontaminated village samples. The leaves which uptake salts directly from the soil also showed higher concentration of heavy elements compared to those of the village samples. As far as flower part was concerned, the elemental concentration was almost similar irrespective of where the cauliflower had been grown. This suggests that there might be a controlled regulatory mechanism for the accumulation of elements in the flower which serves as storage house for plants.

References

[1] J H Scofield, Lawrence Livermore Laboratory UCRL-51326 (1973)
[2] M O Krause, *J. Phys. Chem. Ref. Data* **8**, 307 (1979)
[3] J L Campbell and J X Wang, *Atomic Data Nucl. Data Tables* **43**, 281 (1989)
[4] U Werner and W Jitschin, *Phys. Rev.* **A38**, 4009 (1988)
[5] S Puri, D Mehta, B Chand, N Singh and P N Trehan, *X-Ray Spectrom.* **22**, 358 (1993)
[6] J H Scofield, *At. Data Nucl. Data Tables* **14**, 121 (1974)
[7] B E Gnade, R A Braga and R W Fink, *Phys. Rev.* **C21**, 2025 (1980)
[8] J L Campbell, P L McGhee, R R Gingerich, R W Ollerhead and J A Maxwell, *Phys. Rev.* **A30**, 161 (1984)
[9] A L Catz, *Phys. Rev.* **A40**, 4977 (1989)
[10] A L Catz, *Phys. Rev.* **A36**, 3155 (1987)

[11] S Santra, D Mitra, M Sarkar, D Bhattacharya, P Sen and A C Mandal, *Phys. Rev.* **A69**, 024701 (2004)
[12] W Jitschin, G Materlik, U Werner and P Funker, *J. Phys.* **B18**, 1139 (1985)
[13] U Werner and W Jitschin, *Phys. Rev.* **A38**, 4009 (1988)
[14] E Öz, N Ekinci, Y Özdemir, M Ertugrul, Y Sahin and H Erdogan, *J. Phys.* **B34**, 631 (2001)
[15] M H Chen, B Crasemann and V O Kostroun, *Phys. Rev.* **A4**, 1 (1971)
[16] D Mitra, M Sarkar, D Bhattacharya and L Natarajan, *X-Ray Spectrom.* **37**, 585 (2008)
[17] K S Kahlon, K Shatendra, K L Allawadhi and B S Sood, *Pramana – J. Phys.* **35**, 105 (1990)
[18] K S Kahlon, H S Aulakh, N Singh, R Mittal, K L Allawadhi and B S Sood, *J. Phys.* **B23**, 2733 (1990)
[19] K S Kahlon, H S Aulakh, N Singh, R Mittal, K L Allawadhi and B S Sood, *Phys. Rev.* **A43**, 1455 (1991)
[20] K S Kahlon, N Singh, R Mittal, K L Allawadhi and B S Sood, *Phys. Rev.* **A44**, 4379 (1991)
[21] M Ertuğrul, E Büyükkasap, A Küçükönder, A L Kopya and H Erdoğan, *Nuovo Cimento* **17**, 993 (1995)
[22] M Ertuğrul, E Büyükkasap and H Erdoğan, *Nuovo Cimento* **18**, 671 (1996)
[23] M Ertuğrul, *Nucl. Nstr. & Methods* **B119**, 345 (1996)
[24] L Demir, M Şahin, Ö Söğüt and Y Şahin, *Rad. Phys. Chem.* **59**, 355 (2000)
[25] S Seven and K Koçak, *J. Phys.* **B34**, 2021 (2001)
[26] S Seven and K Koçak, *X-ray Spectrom.* **31**, 75 (2002)
[27] L Demir, M Şahin, Y Kurucu, A Karabulut and Y Şahin, *Rad. Phys. Chem.* **67**, 605 (2003)
[28] S Seven, *Rad. Phys. Chem.* **69**, 451 (2004)
[29] T Papp and J L Campbell, *J. Phys.* **B25**, 3765 (1992)
[30] S Puri, D Mehta, J S Shahi, M L Garg, N Singh and P N Trehan, *Nucl. Instrum. Methods* **B152**, 19 (1999)
[31] D Mehta, S Puri, N Singh, M L Garg and P N Trehan, *Phys. Rev.* **A59**, 2723 (1999)
[32] A Kumar, S Puri, D Mehta, M L Garg and N Singh, *J. Phys.* **B32**, 3701 (1999)
[33] A Kumar, M L Garg, S Puri, D Mehta and N Singh, *X-Ray Spectrom.* **30**, 287 (2001)
[34] H Yamaoka, M Oura, K Takahiro, N Takesima, K Kawatsura, M Mizumaki, U Kleiman, N M Kabachnik and T Mukoyama, *Phys. Rev.* **A65**, 062713 (2002)
[35] H Küst, U Kleiman and W Mehlhorn, *J. Phys.* **B36**, 2073 (2003)
[36] A Tartari, C Baraldi, E Casnati, A D Re, J Fernandez and S Taioli, *J. Phys.* **B36**, 843 (2003)
[37] E G Berezhko, N M Kabachnik and V S Rostovsky, *J. Phys.* **B11**, 1749 (1978)
[38] S Santra, D Mitra, M Sarkar and D Bhattacharya, *Phys. Rev.* **A75**, 022901 (2007)
[39] J H Hubbell, W M J Veigele, E A Briggs, R T Brown, D T Cromer and R Howerton, *J. Phys. Chem. Ref. Data* **4**, 471 (1975); **6**, 615(E) (1977)
[40] J H Hubbell and I Øverbø, *J. Phys. Chem. Ref. Data* **8**, 69 (1979)
[41] D Schaupp, M Schumacher, F Smend, P Rullhusen and J H Hubbell, *J. Phys. Chem. Ref. Data* **12**, 467 (1983)
[42] D T Cromer and D A Liberman, *J. Phys. Chem.* **53**, 1891 (1970)
[43] D T Cromer and D A Liberman, *Acta Crystallogr.* **A37**, 267 (1981)
[44] B Henke, P Lee, T J Tanaka, R Shimabukuro and B Fujikawa, *At. Data Nucl. Data Tables* **27**, 1 (1982)
[45] B L Henke, E M Gullikson and J C Davis, *At. Data Nucl. Data Tables* **54**, 181 (1993)
[46] D T Cromer and D A Liberman, *J. Phys. Chem.* **53**, 1891 (1970)
[47] D T Cromer and D A Liberman, *Acta Crystallogr.* **A37**, 267 (1981)
[48] B Henke, P Lee, T J Tanaka, R L Shimabukuro and B K Fujikawa, *At. Data Nucl. Data Tables* **27**, 1 (1982)
[49] C Bui and M Milazzo, *Nuovo Cimento* **11**, 655 (1989)

[50] A C Mandal, D Mitra, M Sarkar and D Bhattacharya, *Phys. Rev.* **A66**, 042705 (2002)
[51] M Jung, R W Dunford, D S Gemmell, E P Kanter, B Kraessig, T W LeBrun, S H Southworth, L Young, J P L Carney, L LaJohn, R H Pratt and P M Bergstrom Jr, *Phys. Rev. Lett.* **81**, 1596 (1998)
[52] A C Mandal, M Sarkar and D Bhattacharya, *Eur. Phys. J. AP* **17**, 81 (2002)
[53] A C Mandal, S Santra, D Mitra, M Sarkar, D Bhattacharya and S B Majumder, *Ind. J. History of Science* **38**, 351 (2003)
[54] S Santra, G Sengupta, D Bhattacharya, M Sarkar, P K Mitra, D Mitra and P K Chattopadhyay, *Ind. J. History of Science* **43**, 29 (2008)
[55] C J Spark, *Adv. X-ray Anal.* **19**, 18 (1975)
[56] R D Giauque, F S Goulding, J M Jaklevic and R H Pehl, *Anal. Chem.* **45**, 671 (1973)
[57] Quantitative X-ray Analysis System, IAEA Manual, 2005. Doc. Ver.2.0 IAEA (Vienna)
[58] D Gupta, J M Chatterjee, R Ghosh, A K Mitra, S Roy and M Sarkar, *Appl. Rad. Isotopes* **65**, 512 (2007)
[59] D Gupta, J M Chatterjee, R Ghosh, A K Mitra, S Roy and M Sarkar Jr, *Radioanal. Nucl. Chem.* **274**, 389 (2007)
[60] G Mathe-Gaspar and A Anton, *Acta Biol. Szegediensis* **46**, 113 (2002)
[61] H R Verma, *J. Phys.* **B33**, 3407 (2000)